Prime modes of fluid circulation in large-aspect-ratio turbulent Rayleigh-Bénard convection

Jos Verdoold,[1,*] Mark J. Tummers,[1] and Kemo Hanjalić[1,2]
[1]*Department of Multi-Scale Physics, Delft University of Technology, Lorentzweg 1, 2628 CJ Delft, The Netherlands*
[2]*Department of Mechanics and Aeronautics, University of Rome "La Sapienza," Via Edudossiana 18, 00184 Rome, Italy*
(Received 2 April 2009; revised manuscript received 20 July 2009; published 29 September 2009)

Based on a detailed experimental investigation in an aspect-ratio-4 rectangular cell in the range $3.7\times10^7 \leq \mathrm{Ra} \leq 3.7\times10^9$, we present evidence of possible scenarios of the long-term dynamics of large-scale circulations (LSC) in bounded large-aspect-ratio turbulent Rayleigh-Bénard convection. Karhunen-Loève analysis of instantaneous velocity fields from long-time particle image velocimetry measurements suggests two different states, but both appear to be produced by a single large-scale flow structure. The measurements provide a three-dimensional picture of LSC in the $\Gamma=4$ cell. A modified scaling relation between the LSC peak frequency ω_p and Ra is proposed.

DOI: 10.1103/PhysRevE.80.037301 PACS number(s): 47.20.Bp, 44.25.+f, 47.27.te

It is widely assumed that a better insight into a broad spectrum of physical phenomena encountered in the Earth's mantle, atmosphere, and oceans, can be gained from better understanding of the structure and dynamics of turbulent Rayleigh-Bénard convection (RBC). This paradigm of thermal convection occurs when a fluid layer between two horizontal plates is sufficiently heated from below and cooled from above. We recall that RB convection is characterized by the Rayleigh number $\mathrm{Ra}=\alpha g\Delta\Theta H^3/(\nu\kappa)$, and the Prandtl number $\mathrm{Pr}=\nu/\kappa$, where α is the thermal expansion coefficient, $\Delta\Theta$ is the temperature difference between the cold and the hot plate, H is the vertical distance between the plates, ν is the kinematic viscosity, and κ is the thermal diffusivity. The generic RBC implies infinite lateral width W, while all experiments consider bounded finite width cells, thus introducing the aspect ratio $\Gamma=W/H$ as an additional parameter next to Ra and Pr.

RBC has been studied thoroughly, but many important questions remain unanswered [1–4]. In particular, the heat transfer scaling for high Ra numbers and the structure and dynamics of the large-scale circulation (LSC) are topics of intense research [5–7]. Both topics are closely related since the LSC affects the heat transfer.

Most information on the LSC has been deduced from experiments in cells with aspect ratios around $\Gamma=1$ where generally the LSC appears in the form of a single roll spanning over the entire cell with a nearly vertical circulation plane that meanders in azimuthal direction [8–11]. However, it is questionable whether insights gained for such small aspect ratios are relevant to the generic RBC problem, or to practical situations which are often laterally unbounded. The experiments of Niemela and Sreenivasan [5] in a (cylindrical) $\Gamma=4$ cell for Ra numbers between 10^8 and 2×10^{13} suggested indeed that the LSC consists of a single roll also for $\Gamma=4$, but direct evidence in terms of velocity or temperature field, was not presented. Wu and Libchaber [12] performed measurements in a $\Gamma=6.7$ cell and Funfschilling *et al.* [13] carried out heat transfer measurements in cylindrical water-filled cells with Γ varying between 1 and 6. They noticed a small but systematic effect of the aspect ratio on the heat transfer. Recently, Xi and Xia [14,15] have reported on the LSC in RB cells with $\Gamma<1$. For $\Gamma=1/2$ the LSC was found to have a single roll structure for most of the time although a counter-rotating double roll also occurred for brief periods. An interesting aspect of the work by Xi and Xia [14] is the direct measurement of the LSC through planar velocity measurements with particle image velocimetry (PIV).

The current work focuses on the structure and dynamics of the LSC in a $\Gamma=4$ cell. PIV was used to directly measure the flow field for a range of Ra numbers between 3.7×10^7 and 3.7×10^9. The obtained data sets each contain about 2×10^4 individual PIV image pairs (acquired at 1 Hz), which were subsequently analyzed using Karhunen-Loève (K-L) decomposition to determine the most energetic modes and their time dynamics.

The experiments were conducted in a $600\times600\times155$ mm^3 ($W\times W\times H$) water-filled cell, see also [16]. Two hollow 9 mm copper plates at the top and bottom are kept at constant temperatures by passing water from two basins containing constant temperature water (inaccuracy less than 0.03 K) through the plates internal channels. The plates thus impose a controlled temperature difference $\Delta\Theta$ on the working fluid. The side walls are made of 10-mm-thick glass to allow optical access. A Cartesian coordinate system with its origin at the center of the bottom wall is adopted with the x and y coordinates being parallel to the side walls and the z coordinate denoting the wall-normal distance.

Instantaneous velocity fields were measured by using a PIV system that included a Continuum Minilite double-pulsed Nd:YAG laser with a pulse energy of 2×25 mJ. This laser produced an approximately 1-mm-thick light sheet that illuminated the seeding particles (10 μm diameter). Two PCO Sensicam cameras with a resolution of 1280×1024 pixels recorded images of the seed particles in the light sheet. A 28 mm focal length lens with a numerical aperture $f^{\#}=4$ was mounted on each PCO camera. The time separation between pulses varied between 30 and 90 ms depending on Ra. The image pairs were analyzed in three subsequent steps consisting of (adaptive) cross correlation, Gaussian local median filtering, and interpolation. The final interrogation area was 16×16 pixels, corresponding to an area in the measurement plane of 0.4×0.4 cm^2.

*j.verdoold@tudelft.nl

To extract the most dominant flow structures Karhunen-Loève (K-L) decomposition of the velocity field is made using the "method of snapshots" [17–19]. The velocity field is expanded into a finite series of N orthogonal basis functions $\phi_n(\mathbf{x})$ and independent dimensionless coefficients $a_n(t)$,

$$\mathbf{u}(\mathbf{x},t) = \sum_{n=0}^{N-1} a_n(t)\phi_n(\mathbf{x}). \tag{1}$$

Both $\phi_n(\mathbf{x})$ and $a_n(t)$ are uncorrelated and statistically orthogonal. When applied to subsequent instantaneous snapshots, solving $a_n(t)$ can be reduced to solving the eigenvalue problem

$$\int_T C(t,t')a_n(t')dt' = \lambda_n a_n(t), \tag{2}$$

where the two-point correlation tensor C is defined as $C(t,t')=\frac{1}{T}\int\int\int_V \mathbf{u}(\mathbf{x},t)\cdot\mathbf{u}(\mathbf{x},t')d\mathbf{x}$ and λ_n denote the eigenvalues. The spatial basis function belonging to $a_n(t)$ is obtained from

$$\phi_n(\mathbf{x}) = \frac{1}{T\lambda_n}\int_T a_n(t)\mathbf{u}(\mathbf{x},t)dt. \tag{3}$$

Because of the orthogonality of the basis functions, the energy contribution of each mode adds up to the total energy of the flow field, $E=\Sigma_{i=1}^{N_T}\lambda_i$, where N_T denotes the total number of eigenmodes. The large-scale flow structures are deduced by summing the largest eigenvalues. The mode ϕ_0 represents the ensemble average of all instantaneous velocity fields. For this reason ϕ_0 is called the "steady" mode while the higher modes are known as the fluctuating modes. For RBC such a procedure has been performed earlier by [20–24] for numerical simulations of RBC at low Rayleigh number (Ra $\sim 5\times 10^4$).

Long-time PIV measurements ($\approx 2\times 10^4$ s) have been conducted in the $y=0$ plane of the cell for twelve Ra numbers between 3.7×10^7 and 3.7×10^9. In this Ra-number range the Prandtl number varied between 5 and 7. Non-Boussinesq effects did not play a significant role as $\Delta\Theta < 10$ K (Ra$<5\times 10^9$) for all Ra numbers considered in this experiment.

The four most energetic modes of the K-L analysis for Ra$=3.9\times 10^7$ are depicted in descending order in Fig. 1. Streamlines are plotted to indicate the flow structures. The steady mode, ϕ_0, consists of two counter-rotating cells that are nearly symmetric with respect to the y,z plane. The time series for $a_0(t)$ shows that there was no change in direction for any significant period during the 19 000 s measurement. The fluctuating modes ϕ_1 to ϕ_3 indicate an increasing number of rolls. At Ra$\sim 10^7$ the most energetic fluctuating modes appear to be regular rolls. For higher K-L modes, i.e., from ϕ_4 onward, small scale structures resembling intermittent plumes become dominant, while regular rolls patterns are no longer observed.

Figures 2 and 3 show the results of the K-L decomposition for two repeated experiments at Ra$=6\times 10^8$. For these Ra numbers a single roll encompassing the entire width of the RB cell has emerged as the steady mode ϕ_0. This is consistent with the results of earlier PIV experiments reported in [25] that showed that the mean wind sets in for Ra$>10^8$. From the analysis of the fluctuating modes in Figs. 2 and 3 it appeared that two different sets of modes can occur suggesting two different flow patterns. The first type is depicted in Fig. 2. In that case the higher order modes have an increasing number of rolls not dissimilar to the rolls seen in Fig. 1. For the fluctuating modes ϕ_2 and ϕ_3, the flow in between the roll centers is inclined because the centers are not at the same height above the plate. This is in contrast to the situation for the lower Rayleigh number (Fig. 1) where the fluid appears to rise (or fall) more or less vertically in between the cell centers.

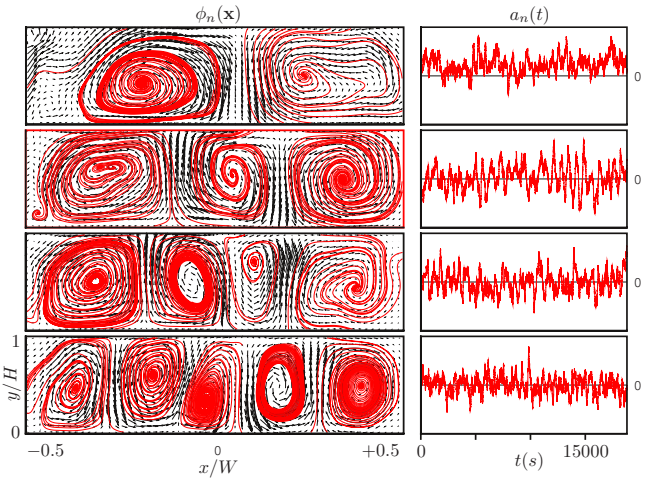

FIG. 1. (Color online) Spatial basis functions ϕ_n (left) and corresponding coefficients $a_n(t)$ (right) for the four most dominant K-L modes for Ra$=3.9\times 10^7$, $n=0,1,2,3$ (top-to-bottom). The depicted modes jointly contain 35% of the total energy in the system. The steady mode ϕ_0 contains 11% of the total energy.

Figure 3 depicts the other set of modes (type II). In this case the fluctuating modes ϕ_1 and ϕ_2 are diagonal flow pat-

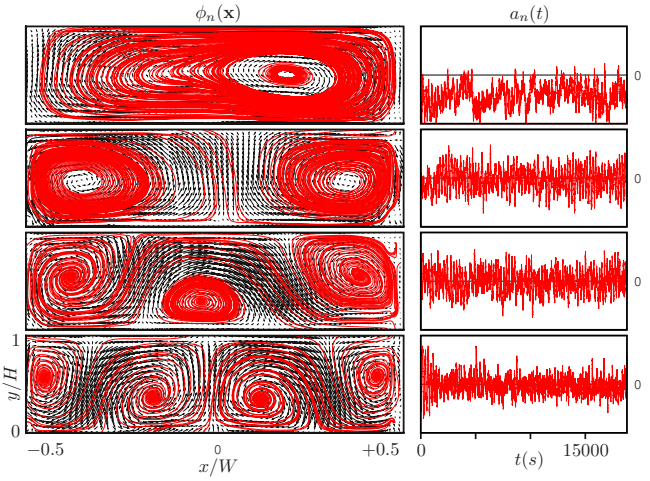

FIG. 2. (Color online) "Type I" spatial basis functions ϕ_n (left) and corresponding coefficients $a_n(t)$ (right) for the four most dominant K-L modes at Ra$=6.2\times 10^8$, $n=0,1,2,3$ (top-to-bottom). The depicted modes jointly contain 41% of the total energy in the system, whereas the steady mode ϕ_0 contains 17% of the total energy.

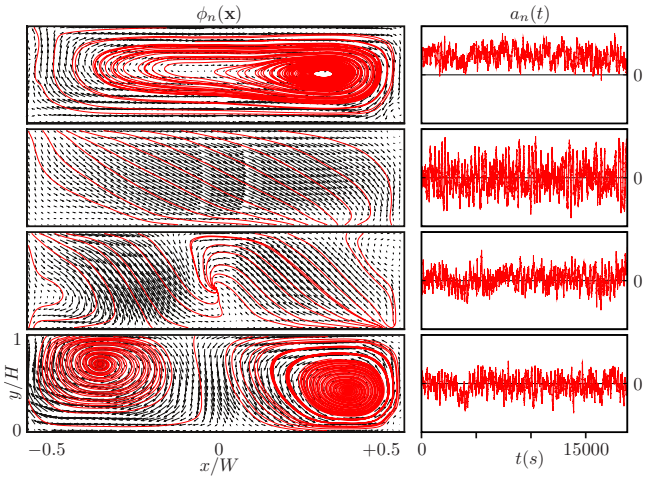

FIG. 3. (Color online) "Type II" spatial basis functions ϕ_n (left) and corresponding coefficients $a_n(t)$ (right) for the four most dominant K-L modes at Ra=5.9×10^8, $n=0,1,2,3$ (top-to-bottom). The depicted modes jointly contain 50% of the total energy in the system, whereas the steady mode ϕ_0 contains 26% of the total energy.

terns. The steady mode ϕ_0 takes a larger share of the total energy than the steady mode for type I. It is interesting that the time series for $a_1(t)$ changes sign in a strongly periodic manner for both types of modes. We argue that the two sets of modes are produced by the same flow structure and expect the same pattern if data from the repeated experiments are rotated by $\pm90°$ around the z axis. At the start up of the RBC this flow structure locks in a certain orientation and then appears at the fixed PIV plane as either a type I or a type II flow pattern. It may even be possible that the flow structure rotates during an experiment but this did apparently not happen during the measurements here presented.

Both sets of modes shown in Figs. 2 and 3 appear randomly in repeated experiments at the same Ra number. Reversals or cessations of the flow are not involved in this process as the time series for $a_0(t)$ do not change sign for any significant time during the measurements. Figure 4 sketches a three-dimensional model for the flow structure in the $\Gamma=4$ cell. Plane A shows the counter-rotating rolls corresponding to fluctuating mode ϕ_1 for type I. Plane B shows the steady mode ϕ_0 (dashed line) and the first fluctuating mode (thick line) for type II. As mentioned earlier the mean wind is strongest in plane B (type II). Figure 4 also illustrates the effect of the periodicity in the fluctuating mode ϕ_1. As explained in [16], during the first phase of the cycle the mean wind is along the circumference of the cell with groups of plumes moving up (or down) along the side walls. However, there are also groups of plumes moving up long before reaching the side wall along an "ascending diagonal" in plane B [Fig. 4 (top)]. The latter flow induces the counter-rotating cells in plane A. During the second phase the fluid stops moving up along the diagonal. During the third phase the flow along the "descending diagonal" in plane B has set in as sketched in Fig. 4 (bottom). This causes the counter-rotating cells in plane A to reverse direction. During phase four the flow along the descending diagonal looses its strength, and the process repeats itself.

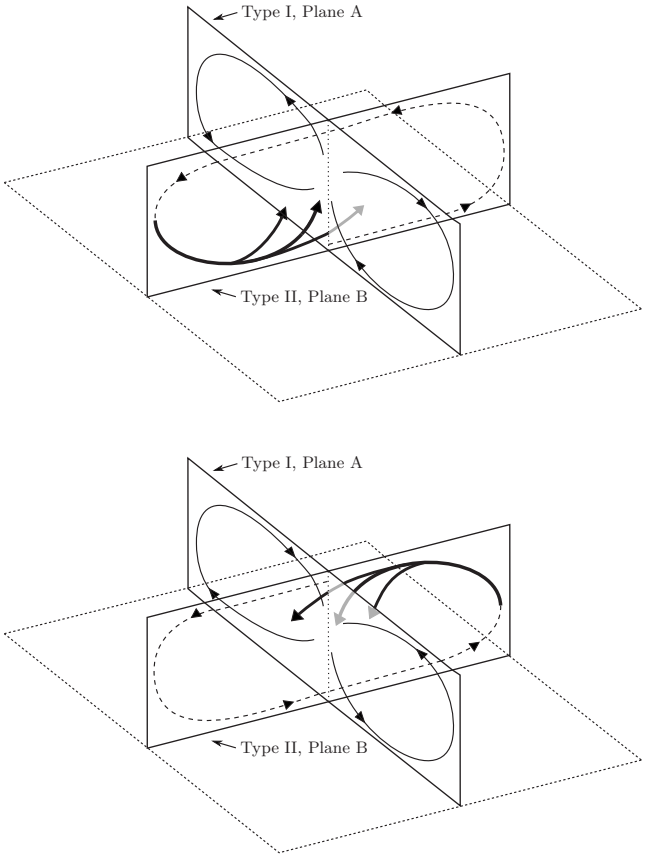

FIG. 4. Schematic of the flow structure in the aspect-ratio-4 cell at two instants in time separated by half a period of the LSC.

The oscillating time series of $a_1(t)$ in Figs. 2 and 3 can be used to determine a power spectrum. The oscillation of the LSC shows up as a peak in this spectrum at a characteristic frequency ω_p. Unlike point measurements from a single PIV

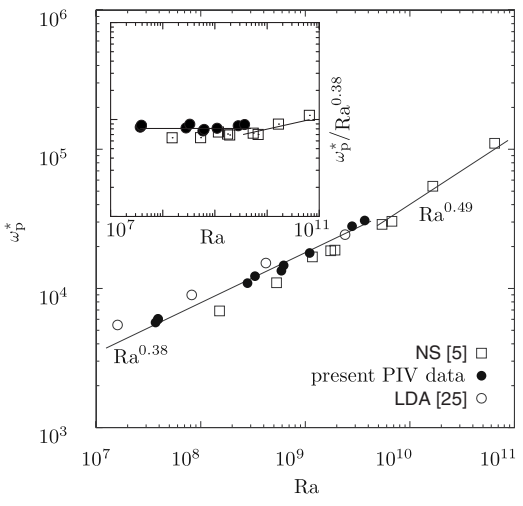

FIG. 5. Dimensionless circular frequency $\omega_p^*=\omega_p H\zeta/\kappa$ as a function of Ra for the present PIV data, compared to data obtained with LDA [25] and to $\Gamma=4$ data from low-temperature helium cells [5] (indicated by NS [5]). A least-squares fit to the K-L data results in the relation $\omega_p^*\sim\mathrm{Ra}^{(0.38\pm0.01)}$. The inset shows the same graph compensated with $\mathrm{Ra}^{0.38}$.

vector, a thermistor or a laser Doppler anemometer (LDA), the $a_1(t)$ time series is calculated using all spatial and temporal information of the instantaneous velocity fields, which effectively increases the statistical reliability of the power spectrum of $a_1(t)$. This is especially important for measurements at relatively low Rayleigh number where characteristic time scales are very large.

The circular frequency ω_p of the oscillating LSC is often scaled with the size of the RBC cell and the diffusion coefficient to enable a comparison with data from other sources [26,27]. Niemela and Sreenivasan [5] use the diagonal of the cell $\zeta=(H^2+W^2)^{1/2}$ to make the circular frequency ω_p dimensionless as in $\omega_p^*=\omega_p H\zeta/\kappa$. Figure 5 shows the ω_p^*-Ra data from the present K-L data together with the data from our earlier LDA measurements [25]. Also shown are the results of an experiment in a $\Gamma=4$ cell operated with helium gas around a temperature of 5 K [5]. A least-squares fit to the K-L data resulted in $\omega_p^* \sim \mathrm{Ra}^{0.38\pm0.01}$. This exponent differs significantly from the 0.48–0.49 reported for other, mostly $\Gamma=1$ experiments, though for significantly higher Ra numbers [8,27–29]. Niemela and Sreenivasan [5] reported that the dependency of ω_p^* on Ra was the same for $\Gamma=1$ and $\Gamma=4$ cells, i.e., $\omega_p^* \sim \mathrm{Ra}^{0.46}$. However, Fig. 5 shows that for $\mathrm{Ra}<10^{10}$ the $\Gamma=4$ data of [5] have an exponent of 0.39 which is nearly equal to that found in the present experiment.

Our experiments show in detail the structure and dynamics and the large-scale flow in thermal convection in square $\Gamma=4$ convection cells. For $\mathrm{Ra}<10^8$ RB convection in this geometry is characterized by isolated rolls. For higher Ra two types of flow patterns consistently appear. Both patterns are consistent with a three-dimensional model of the LSC explaining the observed periodicities of co- and counter-rotating modes. We conjecture that the scenario here described, can be generalized to bounded RB convection for a broader range of high aspect ratios, presumably valid for $\Gamma=3-8$, with the exception of the first mode that may differ for very large Γ.

[1] E. D. Siggia, Annu. Rev. Fluid Mech. **26**, 137 (1994).
[2] E. Bodenschatz, W. Pesch, and G. Ahlers, Annu. Rev. Fluid Mech. **32**, 709 (2000).
[3] L. P. Kadanoff, Phys. Today **54**, 34 (2001).
[4] J. J. Niemela, L. Skrbek, K. R. Sreenivasan, and R. Donnelly, Nature (London) **404**, 837 (2000).
[5] J. J. Niemela and K. R. Sreenivasan, J. Fluid Mech. **557**, 411 (2006).
[6] C. Resagk, R. du Puits, A. Thess, F. Dolzhansky, S. Grossmann, F. F. Araujo, and D. Lohse, Phys. Fluids **18**, 095105 (2006).
[7] E. Brown and G. Ahlers, Phys. Rev. Lett. **98**, 134501 (2007).
[8] X.-L. Qiu and P. Tong, Phys. Rev. E **64**, 036304 (2001).
[9] K. R. Sreenivasan, A. Bershadskii, and J. J. Niemela, Phys. Rev. E **65**, 056306 (2002).
[10] C. Sun, K.-Q. Xia, and P. Tong, Phys. Rev. E **72**, 026302 (2005).
[11] E. Brown and G. Ahlers, J. Fluid Mech. **568**, 351 (2006).
[12] X.-Z. Wu and A. Libchaber, Phys. Rev. A **45**, 842 (1992).
[13] D. Funfschilling, E. Brown, A. Nikolaenko, and G. Ahlers, J. Fluid Mech. **536**, 145 (2005).
[14] H.-D. Xi and K.-Q. Xia, Phys. Rev. E **78**, 036326 (2008).
[15] H.-D. Xi and K.-Q. Xia, Phys. Fluids **20**, 055104 (2008).
[16] J. Verdoold, M. J. Tummers, and K. Hanjalić, Phys. Rev. E **73**, 056304 (2006).
[17] L. Sirovich, Q. Appl. Math. **45**, 561 (1987).
[18] G. Berkooz, P. Holmes, and J. L. Lumley, Annu. Rev. Fluid Mech. **25**, 539 (1993).
[19] Z. Liu, R. J. Adrian, and T. Hanratty, J. Fluid Mech. **448**, 53 (2001).
[20] L. Sirovich and H. Park, Phys. Fluids A **2**, 1649 (1990).
[21] H. Park and L. Sirovich, Phys. Fluids A **2**, 1659 (1990).
[22] L. Sirovich and A. E. Deane, J. Fluid Mech. **222**, 251 (1991).
[23] A. E. Deane and L. Sirovich, J. Fluid Mech. **222**, 231 (1991).
[24] S. M. Zoldi, J. Liu, K. M. S. Bajaj, H. S. Greenside, and G. Ahlers, Phys. Rev. E **58**, R6903 (1998).
[25] J. Verdoold, M. van Reeuwijk, M. J. Tummers, H. J. J. Jonker, and K. Hanjalić, Phys. Rev. E **77**, 016303 (2008).
[26] M. Sano, X. Z. Wu, and A. Libchaber, Phys. Rev. A **40**, 6421 (1989).
[27] J. J. Niemela, L. Skrbek, K. R. Sreenivasan, and R. J. Donnelly, J. Fluid Mech. **449**, 169 (2001).
[28] S. Ciliberto, S. Cioni, and C. Laroche, Phys. Rev. E **54**, R5901 (1996).
[29] X.-L. Qiu, X. D. Shang, P. Tong, and K.-Q. Xia, Phys. Fluids **16**, 412 (2004).